Supporting Information

Synthesis and Characterization of π-extended Triangulene

Shantanu Mishra[†,⊥], Doreen Beyer[‡,⊥], Kristjan Eimre[†], Junzhi Liu[‡], Reinhard Berger[‡], Oliver Gröning[†], Carlo A. Pignedoli[†], Klaus Müllen[‖], Roman Fasel[†,§], Xinliang Feng[‡,*] and Pascal Ruffieux[†,*]

[†]nanotech@surfaces Laboratory, Empa – Swiss Federal Laboratories for Materials Science and Technology, Dübendorf, Switzerland

[‡]Faculty of Chemistry and Food Chemistry, and Center for Advancing Electronics Dresden, Technical University of Dresden, Dresden, Germany

[‖]Department of Synthetic Chemistry, Max Planck Institute for Polymer Research, Mainz, Germany

[§]Department of Chemistry and Biochemistry, University of Bern, Bern, Switzerland

[⊥]These authors contributed equally

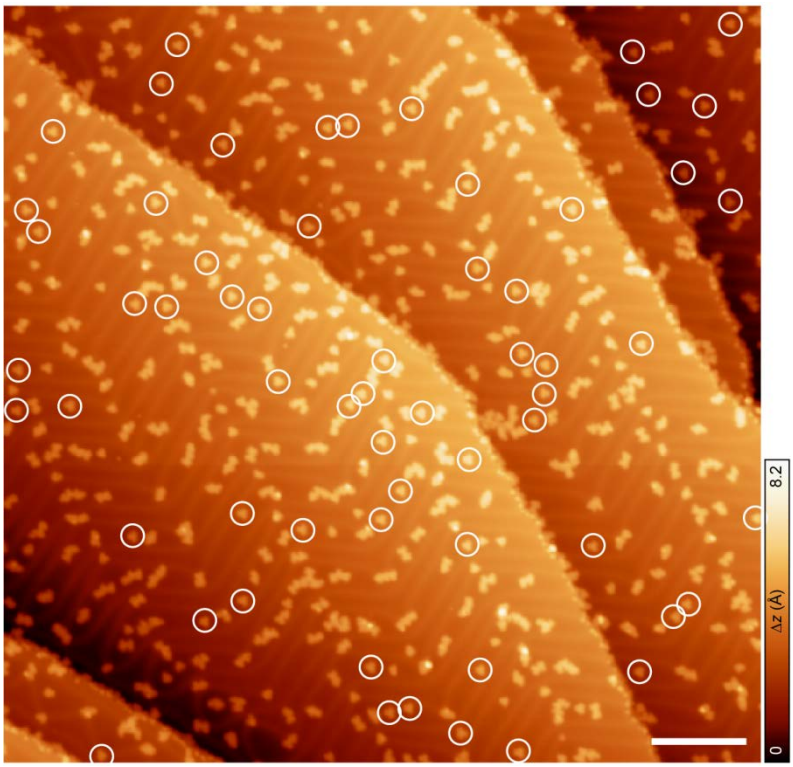

Figure S1. Large-area STM topography image after annealing **2** on Au(111) at 320 °C for 6 minutes (*V* = -600 mV, *I* = 40 pA). White circles highlight individual 3-fold symmetric molecules corresponding to π-extended triangulene (**1**). Scale bar: 15 nm.

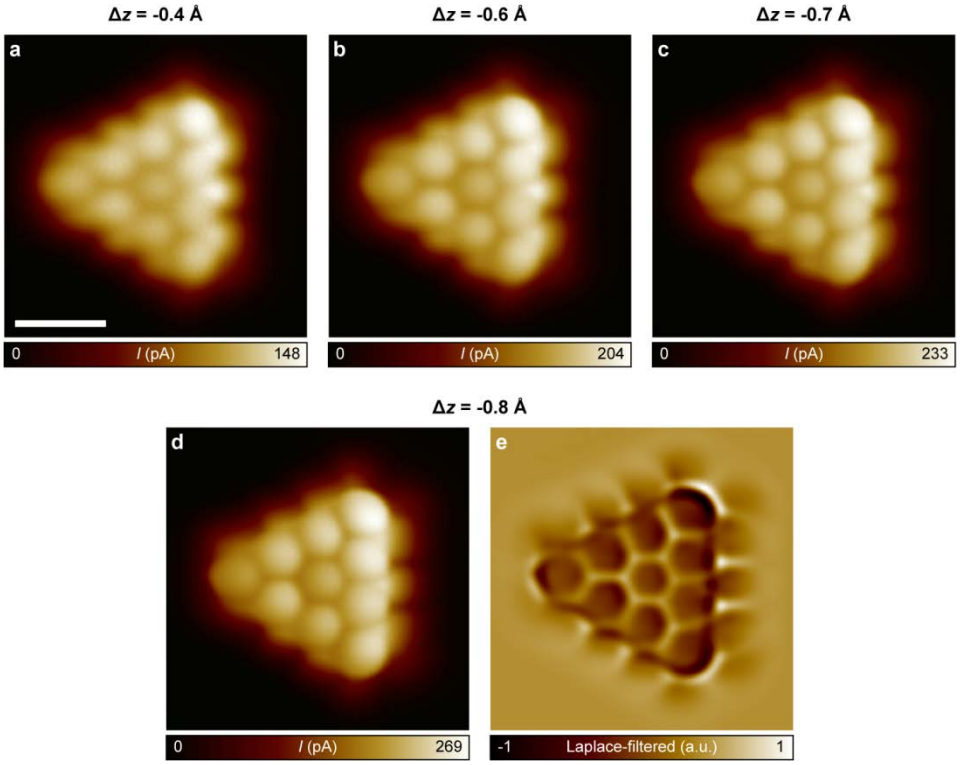

Figure S2. Height-dependent ultrahigh-resolution STM imaging of **1**. (a-d) Series of ultrahigh-resolution STM images of **1** at decreasing tip-molecule distances. (e) Laplace-filtered representation of (d), providing larger chemical structure contrast. For each panel, the lowering of tip height after opening the feedback loop at the center of the molecule (Δ*z*) is indicated at the top. Open feedback parameters: V = -5 mV, I = 50 pA. Scale bar: 0.5 nm.

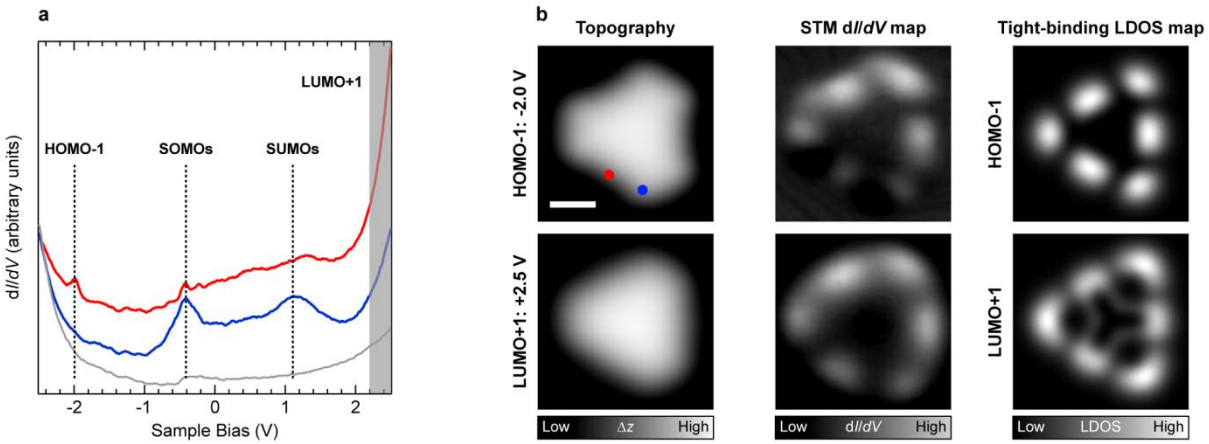

Figure S3. Additional STS measurements on **1**. (a) Long-range d*I*/*dV* spectrum acquired on **1** (red and blue curves) at the positions marked with corresponding colored circles in (b). Gray curve corresponds to reference spectrum acquired on Au(111) (open feedback parameters: V = -2.5 V, I = 350 pA, V_{rms} = 16 mV). Apart from the SOMO and SUMO resonances at -400 mV and +1.15 V, an additional resonance peak is found at -2.0 V. Furthermore, at the positive bias side, there is a significant increase in conductance after approximately +2.0 V. The spectra are vertically offset for visual clarity. (b) Constant-current STM images (left panels) and simultaneously acquired d*I*/*dV* maps (center panels) at -2.0 V and +2.5 V, along with TB-LDOS maps of the HOMO-1 and LUMO+1 of **1** (right panels). The excellent match of the experimental d*I*/*dV* map at -2.0 V and HOMO-1 TB-LDOS map confirms the assignment of the peak at -2.0 V to the HOMO-1 resonance of **1**. Additionally, d*I*/*dV* maps acquired in a bias window between +2.2 V and +2.5 V (region shaded in gray in (a)), with the strongest intensity at +2.5 V, exhibit good correspondence to the LUMO+1 TB-LDOS map. Hence the spectroscopic analyses presented here clearly identify the HOMO-1 and LUMO+1 resonances of **1**. Tunneling parameters for the STM images and associated d*I*/*dV* maps: V = -2.0 V, I = 500 pA (HOMO-1) and V = +2.5 V, I = 450 pA (LUMO+1); V_{rms} = 22 mV. Scale bar: 0.5 nm.

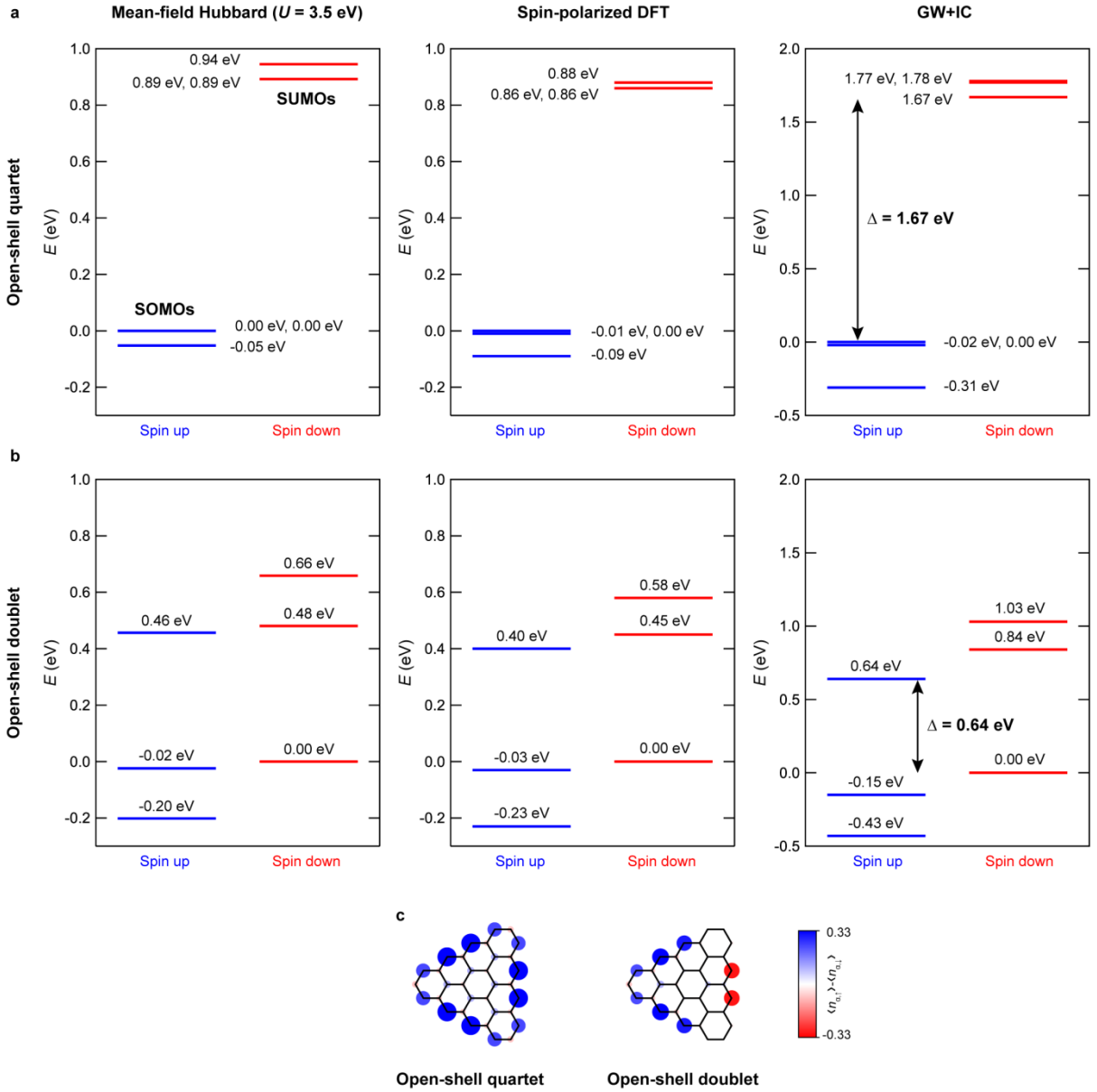

Figure S4. (a, b) Energies of the SOMOs and SUMOs of **1** calculated *via* MFH model (left panels), gas-phase spin-polarized DFT (center panels) and GW method with image charge correction (GW+IC, right panels) for the open-shell quartet (S = 3/2, (a)) and open-shell doublet (S = 1/2, (b)) electronic configurations. Blue and red lines denote spin up and spin down levels. For each panel, the zero of the energy axis has been aligned to the highest-energy SOMO. From both the MFH and DFT level schemes, it is seen that the frontier electronic gap of the open-shell quartet state is about twice as large as for the open-shell doublet state. The experimental Coulomb gap of 1.55 eV determined from STS closely corresponds to the GW+IC frontier gap of 1.67 eV between the quasi-degenerate SOMOs and the non-degenerate SUMO of the open-shell quartet state of **1**. The corresponding GW+IC frontier gap of the open-shell doublet state of **1** is 0.64 eV, which is much lower than the experimental Coulomb gap. This observation strongly suggests that **1** exhibits an open-shell quartet state when adsorbed on Au(111). However, given the broadening of the energy levels of **1** due to adsorption on a metal surface, we cannot unambiguously distinguish between the quasi-degenerate and non-degenerate SOMOs or SUMOs in STS measurements. The rather broad peaks that we obtain experimentally are indicative of the fact that a combined contribution from all three SOMO and SUMO

levels at the respective bias polarities is obtained. (c) Computed MFH spin density distributions of **1** in the open-shell quartet and open-shell doublet configurations.

Supplementary Methods

1. Sample preparation and STM/STS measurements

STM measurements were performed with a commercial low-temperature LT-STM from Scienta Omicron operating at a temperature of 4.5 K and base pressure below 5×10^{-11} mbar. Au(111) single crystal surfaces were prepared *via* iterated cycles of sputtering with Ar^+ ions at a pressure of $p = 6\times10^{-6}$ mbar, and annealing to 750 K for 10 minutes at $p < 1\times10^{-9}$ mbar. Prior to deposition of molecules, the surface quality was checked with STM. Precursor **2** was contained in a quartz crucible and deposited at 393 K from a home-built evaporator on Au(111) surface held at room temperature. Typical sample annealing times after deposition of precursor molecules ranged between 5 and 7 minutes. STM images and d*I*/*dV* maps were acquired in constant-current mode. Unless otherwise noted, gold-coated tungsten tips were used for STM imaging and spectroscopy measurements. Indicated tunneling bias voltages are provided with respect to the sample. d*I*/*dV* spectra and maps were obtained with a lock-in amplifier operating at a frequency of f = 860 Hz, wherein a signal proportional to d*I*/*dV* was obtained from the first harmonic of the tunneling current. Modulation voltages (root mean square amplitude) for individual measurements are provided in the respective figure captions. Ultra-high-resolution STM images were acquired in constant-height mode with CO-functionalized tips, at tunneling biases close to the Fermi energy, and the current signal was recorded. Open feedback parameters and subsequent lowering of the tip height (Δz) for each image are provided in the respective figures/figure captions. CO molecules were deposited on a cold sample (T < 13 K) containing bilayer NaCl(001) islands, and CO-functionalized tips were prepared by picking up individual CO molecules from NaCl islands. The data were processed with Wavemetrics Igor Pro or WSxM[1] software.

2. Calculation methods

2.1. Tight-binding calculations

The tight-binding calculations for **1** have been performed by numerically solving the Mean-Field-Hubbard Hamiltonian with first nearest-neighbor hopping:

$$\hat{H}_{MFH} = -t \sum_{\langle\alpha,\beta\rangle,\sigma} c^{\dagger}_{\alpha,\sigma}\, c^{-}_{\beta,\sigma} + U \sum_{\alpha,\sigma} \langle n_{\alpha,\sigma}\rangle n_{\alpha,\bar{\sigma}} - U \sum_{\alpha} \langle n_{\alpha,\uparrow}\rangle\langle n_{\alpha,\downarrow}\rangle$$

Here, $c^{\dagger}_{\alpha,\sigma}$ and $c^{-}_{\beta,\sigma}$ denote the spin selective ($\sigma \in \{\uparrow,\downarrow\}$) creation and annihilation operator at neighboring sites α and β, t the nearest-neighbour hopping parameter (with t = 2.7 eV used here), U the on-site Hubbard parameter, $n_{\alpha,\sigma}$ the number operator and $\langle n_{\alpha,\sigma}\rangle$ the mean occupation number at site α. Orbital electron densities of the n^{th}-eigenstate with energy E_n have been simulated from the corresponding state vector $a_{n,i,\sigma}$ by:

$$\rho_{n,\sigma}(\vec{r}) = \left| \sum_{i} a_{n,i,\sigma} \phi_{2p_z}(\vec{r} - \vec{r}_i) \right|^2$$

where i denotes the atomic site index and ϕ_{2p_z} denotes the Slater $2p_z$ orbital for carbon.

2.2. DFT and GW calculations

The equilibrium geometry of **1** adsorbed on Au(111) surface was obtained with the CP2K[2] code implementing DFT within a mixed Gaussian plane waves approach.[3] The surface/adsorbate system was modeled within the repeated slab scheme,[4] with a simulation cell containing 4 atomic layers of Au along the [111] direction and a layer of hydrogen atoms to passivate one side of the slab in order to suppress one of the two Au(111) surface states. 40 Å of vacuum was included in the simulation cell to decouple the system from its periodic replicas in the direction perpendicular to the surface. The electronic states were expanded with a TZV2P Gaussian basis set[5] for C and H species and a DZVP basis set for Au species. A cutoff of 600 Ry was used for the plane wave basis set. Norm-conserving Goedecker-Teter-Hutter pseudopotentials[6] were used to represent the frozen core electrons of the atoms. We used the PBE parameterization for the generalized gradient approximation of the exchange correlation functional.[7] To account for van der Waals interactions, we used the D3 scheme proposed by Grimme.[8] The gold surface was modeled by a supercell of 41.27 × 40.85 Å^2 corresponding to 224 surface units. To obtain the equilibrium geometries, we kept the atomic positions of the bottom two layers of the slab fixed to the ideal bulk positions, and all other atoms were relaxed until forces were lower than 0.005 eV/Å. The gas phase unrestricted DFT calculations for the doublet and quartet spin states were performed by optimizing the geometry in a non-periodic cell of 30 × 30 × 20 Å^3 utilizing the Martyna-Tuckerman Poisson solver, while other inputs were kept equivalent to the slab calculation.

CP2K code was also used to perform the eigenvalue-self consistent GW calculations on the isolated molecular geometry corresponding to the adsorption conformation. The calculation was performed based on the unrestricted DFT PBE wavefunctions. We employed the GTH pseudopotentials and analytic continuation with a two-pole model. The aug-DZVP basis set from Wilhelm *et al.*[9] was used. To account for screening by the metal surface, we applied the image charge model.[10] To determine the image plane position with respect to the molecular geometry, we used a distance of 1.42 Å

between the image plane and the first surface layer, as reported by Kharche *et al.*[11] The calculations were performed *via* workflows based on the AiiDA platform.[12]

3. General methods and materials

Unless otherwise noted, all starting chemical materials were purchased from Sigma Aldrich, TCI, Fisher Scientific, ABCR, and other chemical providers. All chemical materials were used as received without further purification. All reactions, unless otherwise described, were carried out under air- and moisture-free conditions using a sealed Schlenk system under argon atmosphere, because of handling air- and moisture-sensitive chemical substances. The reaction progress in solution was monitored by thin layer chromatography (TLC), containing silica-coated aluminum plates and fluorescence marker F_{254} (silica 60, F_{254}, Merck). If necessary, obtained crude reaction products were purified by silica gel chromatography (particle size: 40–63 µm, VWR Chemicals). Proton and carbon nuclear magnetic resonance spectra (^{1}H and ^{13}C-NMR) were recorded at room temperature (296 K) on a BRUKER AC 300 P NMR instrument, operating at 300 MHz for ^{1}H-NMR and 75 MHz for ^{13}C-NMR, or on a BRUKER AV III 600 NMR instrument, operating at 600 MHz for ^{1}H NMR and 151 MHz for ^{13}C NMR. The NMR measurements were carried out in the liquid-state using deuterated dichloromethane as solvent (CD_2Cl_2, 99.8 atom% D, $\delta_{H\text{-}NMR}$ = 5.32 ppm / $\delta_{C\text{-}NMR}$ = 54.2 ppm), purchased from Euroisotop. In addition, for the full structural characterization of compound mixture **2**, 2D-NMR measurements were performed in deuterated tetrachloroethane ($C_2D_2Cl_4$, 99.6 atom% D, $\delta_{H\text{-}NMR}$ = 5.91 ppm / $\delta_{C\text{-}NMR}$ = 73.8 ppm), purchased from Carl Roth GmbH. The 2D-NMR spectra were recorded at 303 K on a Bruker Avance III 500 spectrometer operating at 500 MHz for ^{1}H NMR. The peak pattern is described by commonly used abbreviations: s = singlet, d = doublet, t = triplet and m = multiplet. MALDI-TOF (matrix-assisted laser desorption/ionization) mass spectra (MS) were obtained in the liquid-state on Autoflex Speed MALDI-TOF from BRUKER, using *trans*-2-[3-(4-*tert*-butylphenyl)-2-methyl-2-propenylidene]malononitrile (DCTB) as matrix substrate. High-resolution atmospheric pressure chemical ionization MS (HR-APCI-MS) was recorded with Agilent 6538 Ultra High Definition (UHD) Accurate-Mass Q-TOF LC/MC system. Elemental analysis from recrystallized solid compounds was carried out on a varia MICRO cube from Elementar. Therefore, the solid was burned at 1150 °C for 70 seconds under oxygen supply. The melting points were determined with a Melting Point M-560 machine from BÜCHI. The temperature range was set to 90–340 °C with a temperature interval of 10 °C/min. The measurements were performed in melting point tubes from Marienfeld (80 x 1.5 mm, one-side open) and the melting point temperature was recorded once the sample was completely melted.

4. Synthetic procedures

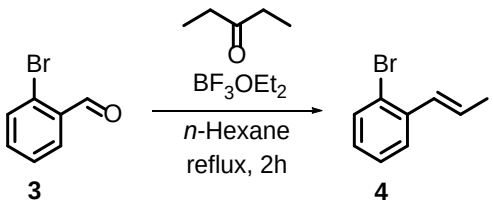

Scheme S1. Synthesis of compound **4**.

(*E*)-1-Bromo-2-(prop-1-enyl)benzene (4): The synthesis of compound **4** was performed in accordance with literature protocol.[13,14] An oven-dried Schlenk flask was charged with commercially available 2-bromobenzaldehyde (**3**) (15.4 g, 83.0 mmol, 1.6 eq.), pentan-3-one (6.46 g, 75.0 mmol, 1.4 eq.) and 100 ml dry *n*-hexane. To the intensively stirred mixture, a solution of boron trifluoride diethyl etherate (BF_3OEt_2) (7.5 g, 53.0 mmol, 1.0 eq.) was added and the mixture was refluxed for 2 hours. After cooling down to room temperature and quenching with water, the aqueous layer was extracted three times with diethyl ether. The combined organic phase was dried over magnesium sulfate. After evaporating the solvent, the crude product was purified by silica gel chromatography using *iso*-hexane as eluent. Compound **4** was obtained as a colorless liquid (10.0 g, 100%).

^{1}H-NMR (CD_2Cl_2, 300 MHz): δ = 7.51 (td, *J* = 8.2, 1.5 Hz, 2H), 7.26 (ddd, *J* = 7.9, 4.3, 0.6 Hz, 1H), 7.12 – 7.02 (m, 1H), 6.73 (dd, *J* = 15.6, 1.7 Hz, 1H), 6.22 (dq, *J* = 15.6, 6.7 Hz, 1H), 1.92 (dd, *J* = 6.7, 1.8 Hz, 3H) ppm. The spectroscopic data are in consistence with those described in literature.[13,14]

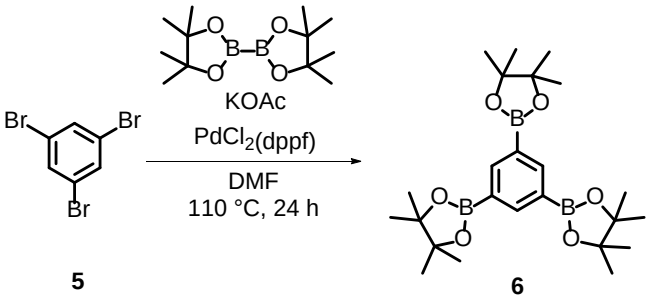

Scheme S2. Synthesis of compound **6**.

1,3,5-Phenyltriboronic acid trispinacol ester (6): The synthesis of compound **6** was performed in accordance with literature protocol.[15] A two-neck round bottom flask was charged with commercially available 1,3,5-tribromobenzene (**5**) (15.0 g, 47.7 mmol, 1.0 eq.) and bis(pinacolato)diboron (38.1 g, 150 mmol, 3.15 eq.). Afterwards, 250 ml dry dimethylformamide (DMF) was transferred to the flask *via* cannula. To the prepared mixture, potassium acetate (KOAc) (28.0 g, 285.9 mmol, 6.0 eq.) and [1,1'-bis(diphenylphosphino)ferrocene]dichloropalladium(II) ($PdCl_2$(dppf)) (0.80 g, 0.9 mmol, 0.1 eq.) were quickly added and the mixture was heated to 110 °C and stirred vigorously for 24 hours. After cooling down to room temperature, the reaction was quenched with 200 ml deionized water. The resulting black precipitate was filtered and washed several times with an excess of water. The crude boronic ester was further purified by a short silica gel pad using ethyl acetate as eluent to remove the remaining residue of catalyst. After solvent evaporation under reduced pressure, the obtained solid was washed with methanol and dried under vacuum. Compound **6** was isolated as a light beige solid (11.3 g, 52%).

^{1}H-NMR (CD_2Cl_2, 300 MHz): δ = 8.22 (s, 3H), 1.34 (s, 36H) ppm. The spectroscopic data are in consistence with those described in literature.[15]

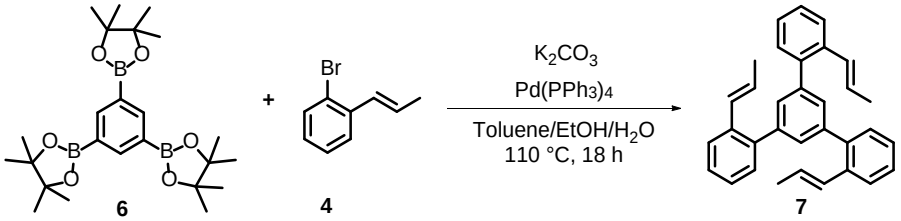

Scheme S3. Synthesis of compound **7**.

2,2''-Di((*E*)-prop-1-en-1-yl)-5'-(2-((*E*)-prop-1-en-1-yl)-1,1':3',1''-terphenyl (7): A solution of 105 ml ethanol (EtOH), 21 ml water (H_2O) and 21 ml toluene was prepared. (*E*)-1-bromo-2-(prop-1-enyl)benzene (**4**) (5.5 g, 27.0 mmol, 3.6 eq.) and compound **6** (3.5 g, 7.0 mmol, 1.0 eq.) were added and the resulting mixture was intensively purged with argon for 30 minutes. Afterwards, potassium carbonate (K_2CO_3) (9.5 g, 69.0 mmol, 9.0 eq.) and tetrakis(triphenylphosphine)palladium(0) ($Pd(PPh_3)_4$) (0.5 g, 0.4 mmol, 0.06 eq.) were added in one portion, and the reaction mixture was maintained at 110 °C for 18 hours. The cold solution was extracted three times with ethyl acetate, washed with brine and dried over magnesium sulfate. The crude product was purified by silica gel chromatography using dichloromethane/*iso*-hexane 1:9 as eluent to afford **7** as a white solid (950 mg, 35%). Further purification by *r*GPC and recrystallization from dichloromethane/methanol affords **7** as colorless crystals.

^{1}H-NMR (CD_2Cl_2, 600 MHz): δ = 7.55 – 7.44 (m, 3H), 7.33 – 7.14 (m, 12H), 6.46 (dd, *J* = 15.7, 1.6 Hz, 3H), 6.11 (dq, *J* = 15.6, 6.6 Hz, 3H), 1.75 (dd, *J* = 6.6, 1.7 Hz, 9H) ppm.

^{13}C-NMR (CD_2Cl_2, 151 MHz): δ = 141.5, 140.7, 136.8, 130.9, 130.5, 130.4, 128.3, 127.6, 127.5, 126.5, 54.20, 19.3 ppm.

HR-APCI Mass (positive mode): calc. for $[M+H]^+$: 427.2347, found for $[M+H]^+$: 427.2424 (deviation: 18.02 ppm).

Elemental analysis $C_{33}H_{30}$: calc. for C: 92.50, H: 6.897; found for C: 92.90, H: 7.09%.

Melting point: 122.6 °C.

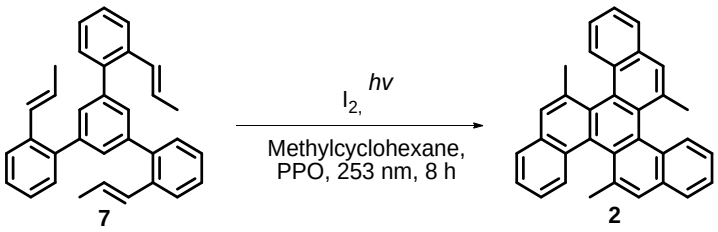

Scheme S4. Synthesis of compound **2**.

5,11,17-Trimethylbenzo[*c*]naphtha[2,1-*p*]chrysene (2): An oven dried sealed quartz tube was charged with **7** (50.0 mg, 0.12 mmol, 1.0 eq.) and iodine (I_2) (92.0 mg, 0.36 mmol, 3.0 eq.). Under argon atmosphere, 100 ml dry methylcyclohexane (MCH) and 1 ml of dry (±)propylene oxide (PPO) were added. The resulting mixture was irradiated with 253 nm light for 8 hours. Afterwards, the reaction was quenched with an aqueous solution of sodium thiosulfate, extracted with ethyl acetate three times, washed with brine and dried over magnesium sulfate. After evaporation of the solvent excess, the crude photoproduct was purified by silica gel chromatography using dichloromethane/*iso*-hexane 1:6 as eluent to afford **2** as a light orange solid (40 mg, 80%). NMR spectroscopy of photoproduct **2** revealed an isomeric mixture. However, liquid-state HR-MALDI-TOF and HR-APCI mass spectrometry support the presumption that the condensed precursor **2** was successfully synthesized. The below listed analysis data were recorded from the isomeric mixture of compound **2**.

^{1}H-NMR (CD_2Cl_2, 300 MHz): δ = 8.22 (d, *J* = 8.2 Hz, 1H), 8.00 (d, *J* = 8.3 Hz, 1H), 7.97 (d, *J* = 7.1 Hz, 1H), 7.95 (s, 1H), 7.90 (s, 1H), 7.78 (s, 1H), 7.59 – 7.55 (m, 2H), 7.55 – 7.49 (m, 2H), 7.47 (t, *J* = 7.0 Hz, 1H), 2.49 (s, 3H), 2.46 (s, 2H) ppm.

^{13}C-NMR (CD_2Cl_2, 75 MHz): δ = 134.2, 133.3, 133.2, 131.6, 130.8, 130.2, 129.2, 128.7, 127.5, 127.3, 126.7, 126.51, 126.3, 125.3, 125.1, 25.6, 25.4 ppm.

HR-MALDI-TOF (matrix: DCTB): calc. for $[M]^+$: 420.1878, found for $[M]^+$: 420.1672 (deviation: 49.0 ppm).

HR-APCI-MS (positive mode): calc. for $[M+H]^+$: 421.1956, found for $[M+H]^+$: 421.1950 (deviation: 1.42 ppm).

Elemental analysis and melting point: not measured due to photoproduct mixture.

5. High-resolution mass spectra (HR-MALDI-TOF-MS, HR-ESI-MS, HR-APCI-MS)

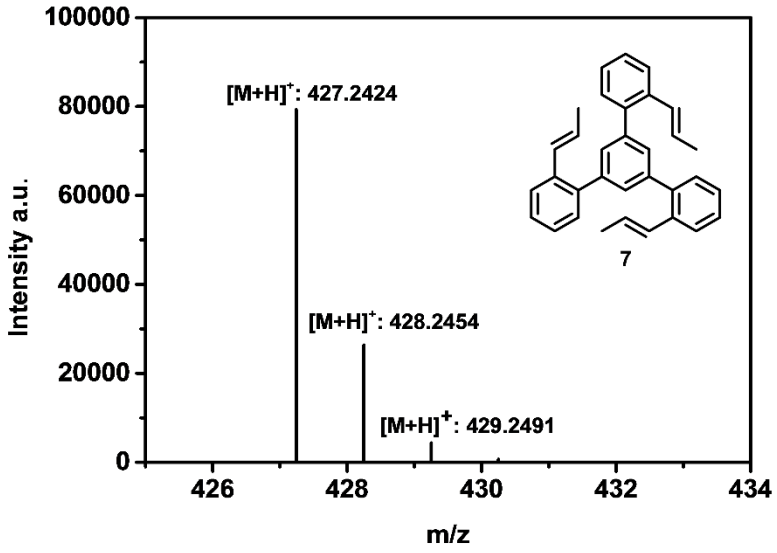

Figure S5. Liquid-state HR-APCI-MS (positive mode) of compound **7**.

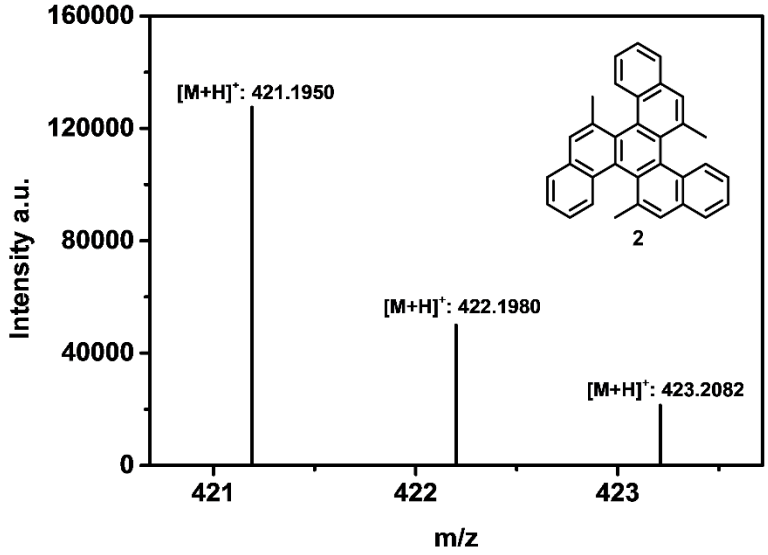

Figure S6. Liquid-state HR-APCI-MS (positive mode) of isomeric mixture **2**.

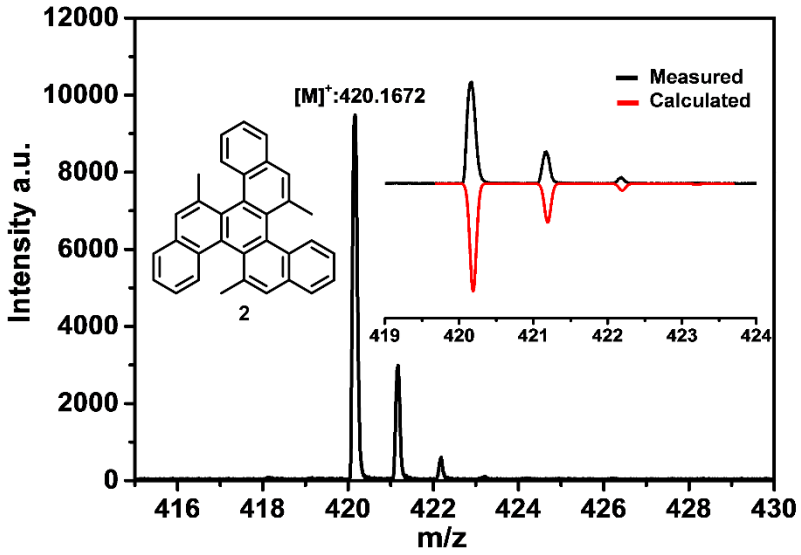

Figure S7. Liquid-state HR-MALDI-TOF of isomeric mixture **2** (matrix: DCTB).

6. NMR Characterization (^{1}H-, ^{13}C- and 2D-NMR)

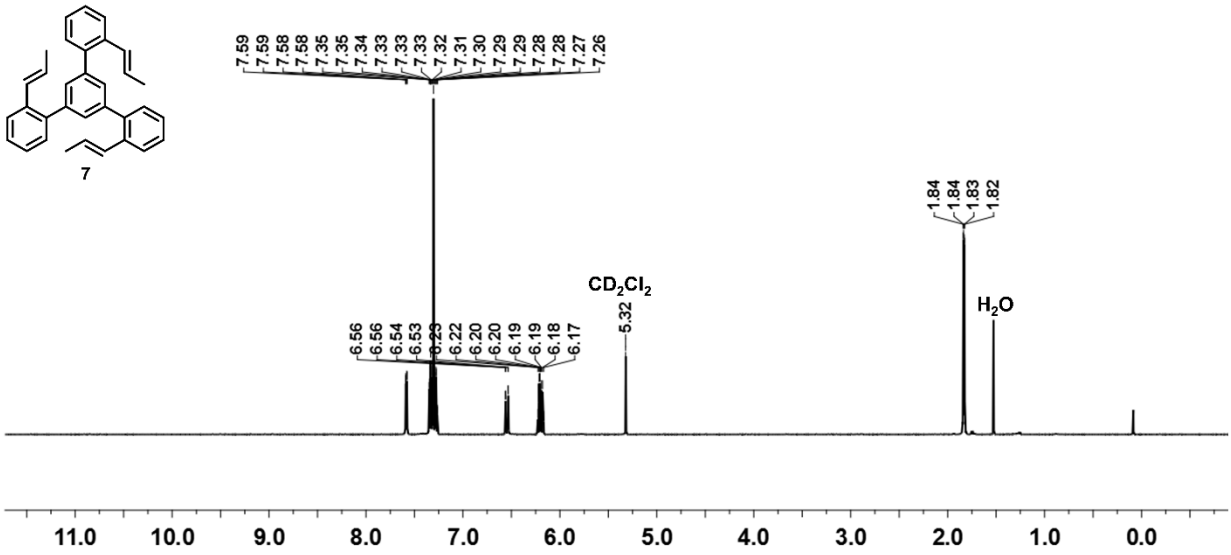

Figure S8. Liquid-state ^{1}H-NMR spectrum of compound **7** measured in CD_2Cl_2 at room temperature. Frequency: 600 MHz.

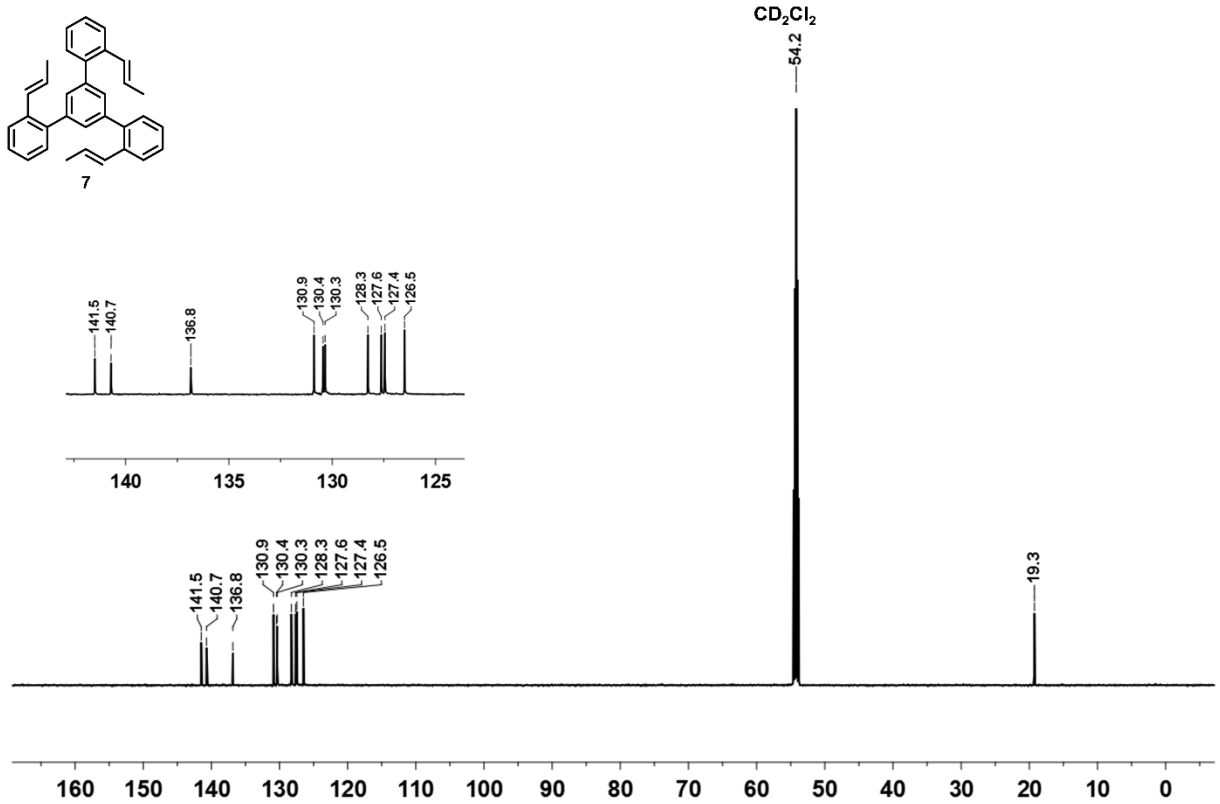

Figure S9. Liquid-state ^{13}C-NMR spectrum of compound **7** measured in CD_2Cl_2 at room temperature. Frequency: 151 MHz.

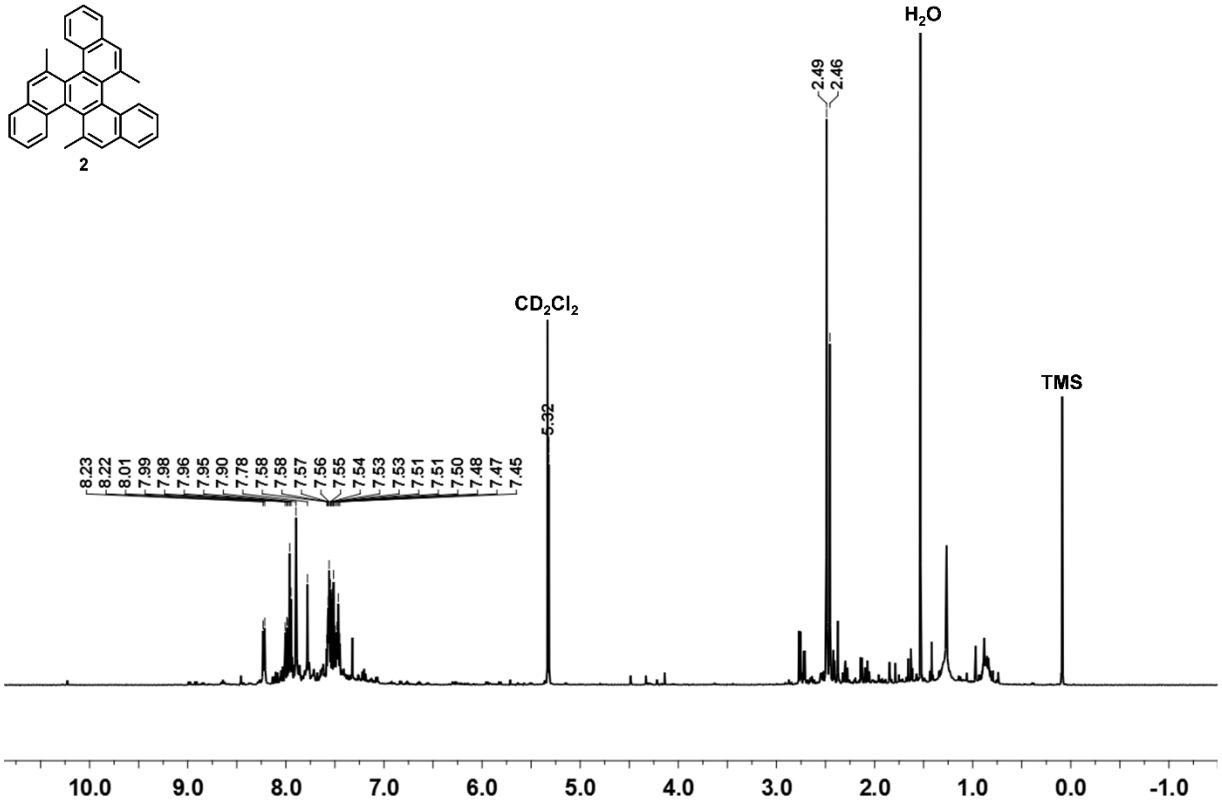

Figure S10. Liquid-state ^{1}H-NMR spectrum of isomeric mixture **2** measured in CD_2Cl_2 at room temperature. Frequency: 300 MHz.

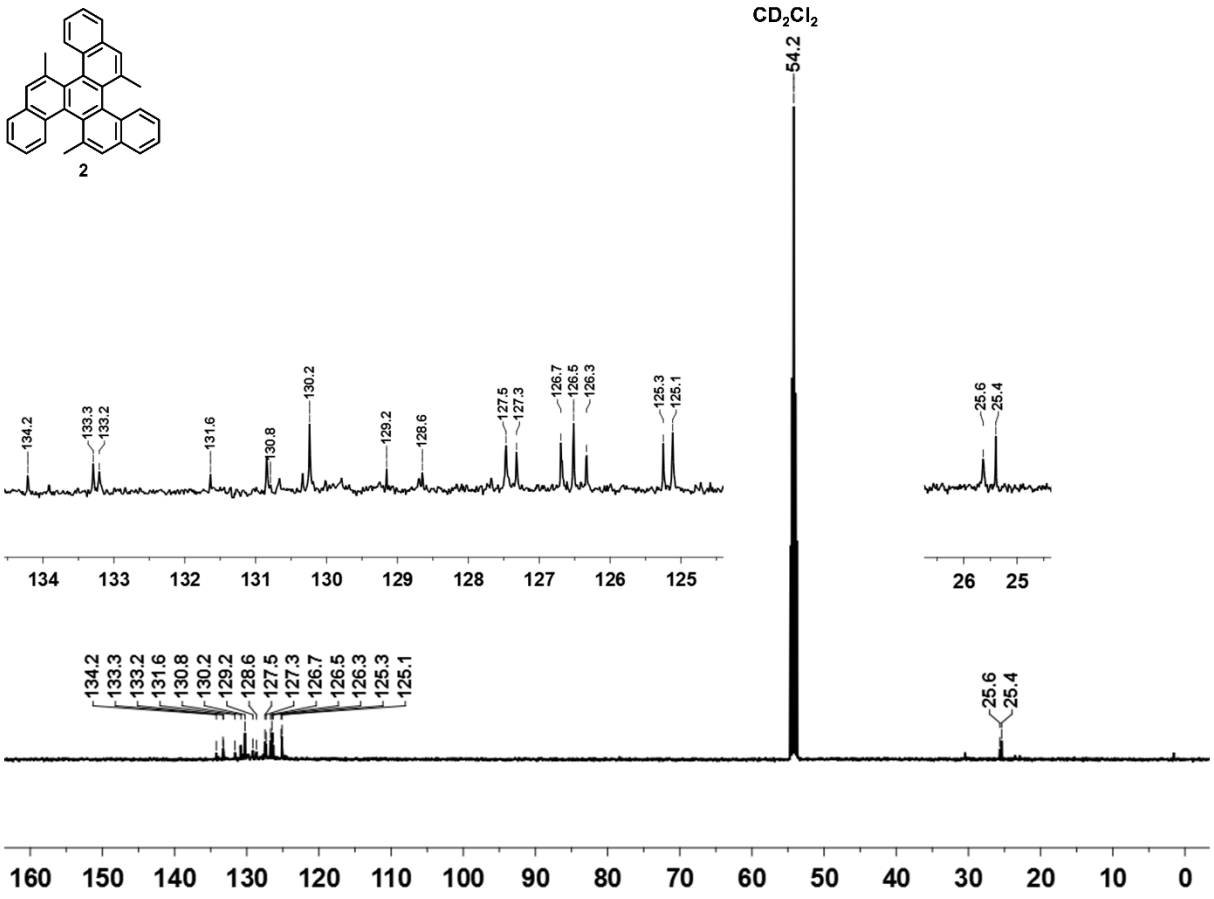

Figure S11. Liquid-state ^{13}C-NMR spectrum of isomeric mixture **2** measured in CD_2Cl_2 at room temperature. Frequency: 75 MHz.

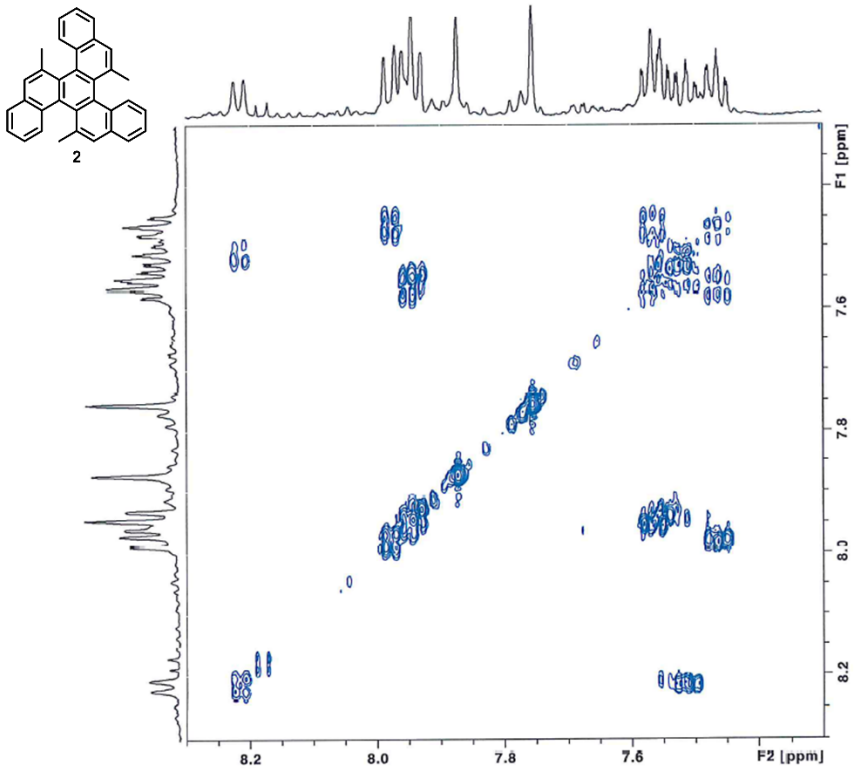

Figure S12. Liquid-state COSY-NMR spectrum of isomeric mixture **2** measured in $C_2D_2Cl_4$ at 303 K. Frequency: 500 MHz.

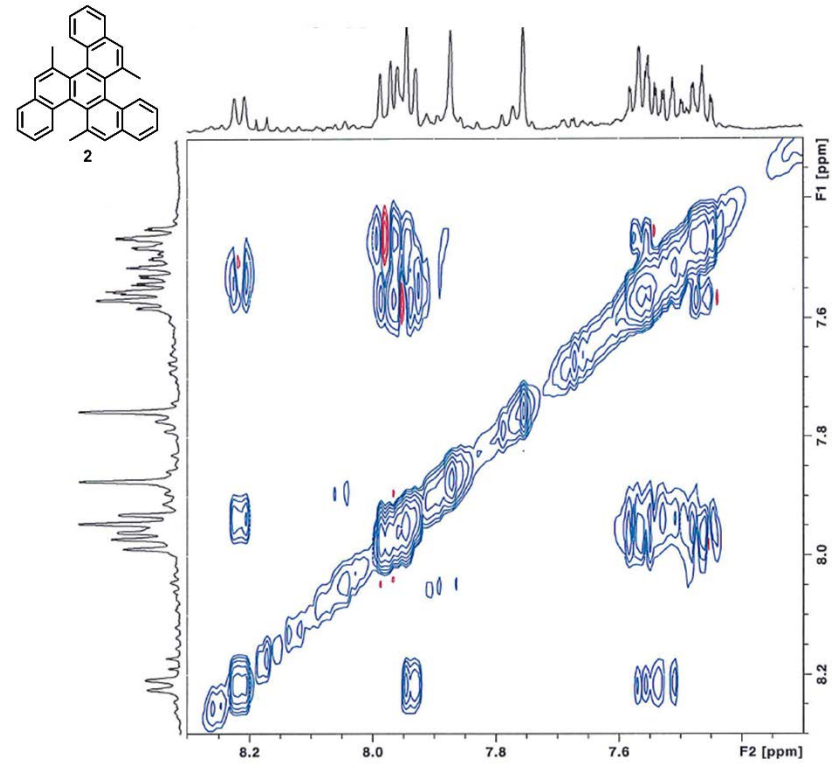

Figure S13. Liquid-state TOCSY-NMR spectrum of isomeric mixture **2** measured in $C_2D_2Cl_4$ at 303 K. Frequency: 500 MHz.

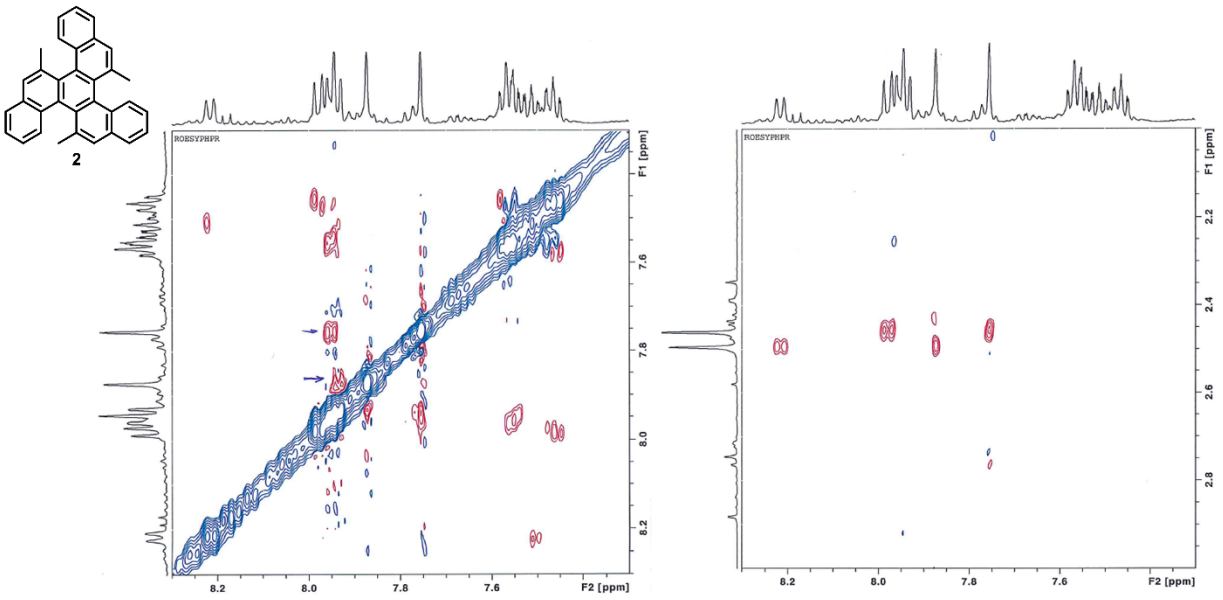

Figure S14. Liquid-state ROESY-NMR spectra of isomeric mixture **2** measured in $C_2D_2Cl_4$ at 303 K. Frequency: 500 MHz.

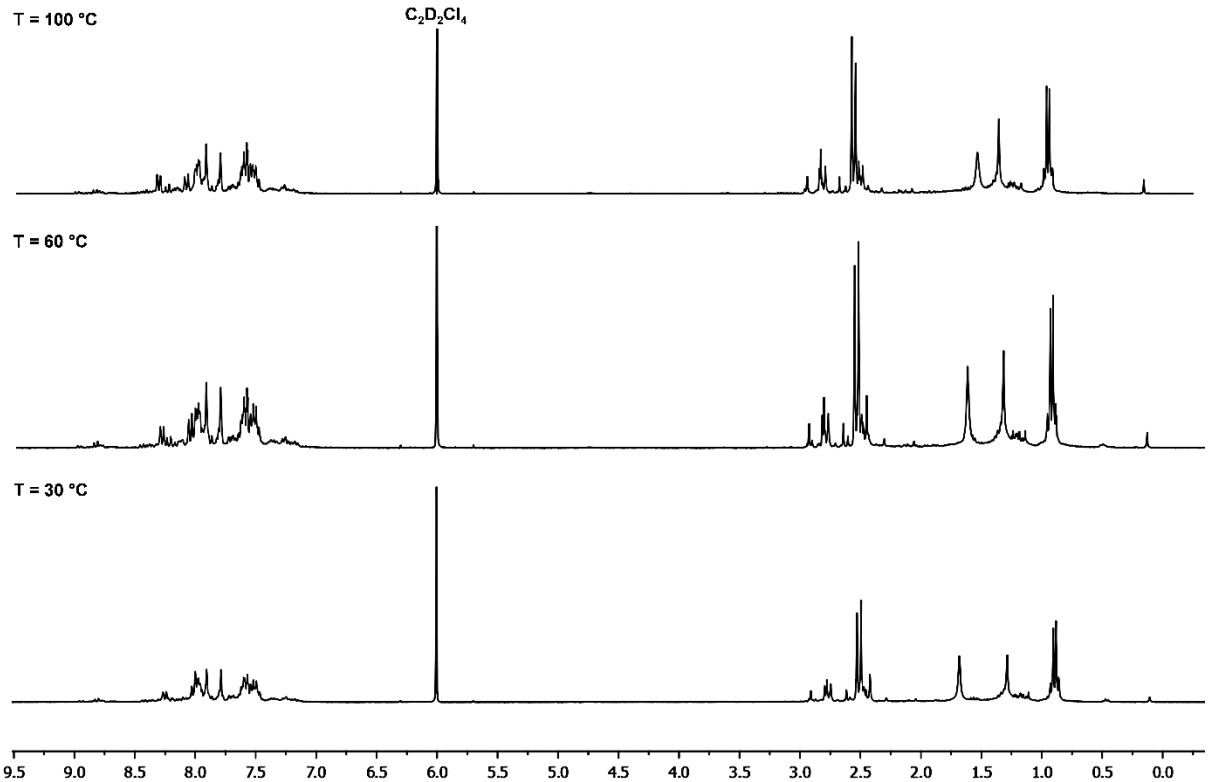

Figure S15. Temperature-dependent ^{1}H-NMR spectra of compound mixture **2** measured in $C_2D_2Cl_4$. Frequency: 300 MHz.

Comments: The temperature-dependent ^{1}H-NMR measurement under argon atmosphere in the range of 30 °C to 100 °C (ΔT = 10 °C) of compound mixture **2** does not afford the intended simplification of

the NMR spectra. The NMR spectra recorded at elevated temperatures, *e.g.* 60 °C and 100 °C, give the same signals and a complete signal assignment is still hampered.

Supplementary References

(1) Horcas, I.; Fernández, R.; Gómez-Rodríguez, J. M.; Colchero, J.; Gómez-Herrero, J.; Baro, A. M. WSXM: A Software for Scanning Probe Microscopy and a Tool for Nanotechnology. *Rev. Sci. Instrum.* **2007**, *78* (1), 013705.

(2) Hutter, J.; Iannuzzi, M.; Schiffmann, F.; Vandevondele, J. Cp2k: Atomistic Simulations of Condensed Matter Systems. *Wiley Interdiscip. Rev. Comput. Mol. Sci.* **2014**, *4* (1), 15–25.

(3) VandeVondele, J.; Krack, M.; Mohamed, F.; Parrinello, M.; Chassaing, T.; Hutter, J. Quickstep: Fast and Accurate Density Functional Calculations Using a Mixed Gaussian and Plane Waves Approach. *Comput. Phys. Commun.* **2005**, *167* (2), 103–128.

(4) Pickett, W. E. Pseudopotential Methods in Condensed Matter Applications. *Comput. Phys. Rep.* **1989**, *9* (3), 115–197.

(5) VandeVondele, J.; Hutter, J. Gaussian Basis Sets for Accurate Calculations on Molecular Systems in Gas and Condensed Phases. *J. Chem. Phys.* **2007**, *127* (11), 114105.

(6) Goedecker, S.; Teter, M.; Hutter, J. Separable Dual-Space Gaussian Pseudopotentials. *Phys. Rev. B* **1996**, *54* (3), 1703–1710.

(7) Lee, C.-C.; Yamada-Takamura, Y.; Ozaki, T. Unfolding Method for First-Principles LCAO Electronic Structure Calculations. *J. Phys. Condens. Matter* **2013**, *25* (34), 345501.

(8) Grimme, S.; Antony, J.; Ehrlich, S.; Krieg, H. A Consistent and Accurate Ab Initio Parametrization of Density Functional Dispersion Correction (DFT-D) for the 94 Elements H-Pu. *J. Chem. Phys.* **2010**, *132* (15), 154104.

(9) Wilhelm, J.; Del Ben, M.; Hutter, J. GW in the Gaussian and Plane Waves Scheme with Application to Linear Acenes. *J. Chem. Theory Comput.* **2016**, *12* (8), 3623–3635.

(10) Neaton, J. B.; Hybertsen, M. S.; Louie, S. G. Renormalization of Molecular Electronic Levels at Metal-Molecule Interfaces. *Phys. Rev. Lett.* **2006**, *97* (21), 216405.

(11) Kharche, N.; Meunier, V. Width and Crystal Orientation Dependent Band Gap Renormalization in Substrate-Supported Graphene Nanoribbons. *J. Phys. Chem. Lett.* **2016**, *7* (8), 1526–1533.

(12) Pizzi, G.; Cepellotti, A.; Sabatini, R.; Marzari, N.; Kozinsky, B. AiiDA: Automated Interactive Infrastructure and Database for Computational Science. *Comput. Mater. Sci.* **2016**, *111*, 218–230.

(13) Takesue, T.; Fujita, M.; Sugimura, T.; Akutsu, H. A Series of Two Oxidation Reactions of Ortho-Alkenylbenzamide with Hypervalent Iodine(III): A Concise Entry into (3R,4R)-4-Hydroxymellein and (3R,4R)-4-Hydroxy-6-Methoxymellein. *Org. Lett.* **2014**, *16* (17), 4634–4637.

(14) Barbasiewicz, M.; Michalak, M.; Grela, K. A New Family of Halogen-Chelated Hoveyda–Grubbs-Type Metathesis Catalysts. *Chem. – Eur. J.* **2012**, *18* (45), 14237–14241.

(15) Zhang, Y.-B.; Furukawa, H.; Ko, N.; Nie, W.; Park, H. J.; Okajima, S.; Cordova, K. E.; Deng, H.; Kim, J.; Yaghi, O. M. Introduction of Functionality, Selection of Topology, and Enhancement of Gas Adsorption in Multivariate Metal–Organic Framework-177. *J. Am. Chem. Soc.* **2015**, *137* (7), 2641–2650.